Stabilization of Oxo-Metal Bonding by the π-Conjugated System in Dithiolate Ligands: *cis*-Dioxotungsten(VI) Bis(naphthalenedithiolato) and the Related Complexes as Models for Tungsten Oxidoreductases

Hiroyuki Oku, Norikazu Ueyama, and Akira Nakamura*

Department of Macromolecular Science, Faculty of Science, Osaka University, Toyonaka, Osaka 560

(Received April 22, 1996)

As a model of tungsten oxidoreductase, a dioxotungsten(VI) dithiolato complex, $(NEt_4)_2$- $[W^{VI}O_2(ndt)_2]\cdot H_2O$ (**1**) (ndt = 2,3-naphthalenedithiolato), was synthesized. It has provided the detailed structural dimensions of mutual *trans* influence between oxo and thiolate. The complex, **1**, crystallizes in space group $P2_1/n$ with $a = 7.396(2)$, $b = 17.581(2)$, $c = 28.839(2)$ Å, $\beta = 95.35(2)$, and $Z = 2$, and was refined to $R = 2.3\%$. The short S–C distances of the thiolate *trans* to the W^{VI}=O groups indicate the presence of the partial double bonding at S–C (thiketone-like) which contributes to the stabilization of the dioxotungsten(VI) species by weakening π-interaction of the W^{VI}–S bonds *trans* to the W^{VI}=O groups. In the tungstopterin cofactor and the molybdopterin cofactor of the enzyme, the double bonding nature of S–C (thioketone-like) is expected to stabilize the oxo ligand of the tungsten and molybdenum ion.

Some new examples of tungsten-containing oxidoreductases, which probably catalyze oxo-transfer reactions, were recently discovered as isolated from thermophilic and hyper thermophilic bacteria.[1—13] ESR and EXAFS has been extensively utilized to reveal the structure of the enzyme active site.[3,6,14—16] Particularly, the EXAFS spectroscopic analysis of oxidized aldehyde-ferredoxin oxidoreductase[15,16] has clearly shown the presence of *cis*-$(W^{VI}O_2)^{2+}$ centers surrounded by sulfur ligand atoms which are similar or very close to the active site of molybdenum oxidoreductases, such as sulfite oxidase.[17] From the tungsten and molybdenum enzymes, a variety of pterin cofactors have been isolated.[18—20] The pterin cofactor generally contains a pterin ring and a dithiolene structure.

Very recently, a crystallographic report by Rees et al. has revealed the *bis*(dithiolene) coordination to tungsten ion in aldehyde ferredoxin oxidoreductase.[21] The reported structure of tungstopterin cofactor closely resembles our model complexes, $Q_2[W^{VI}O_2(bdt)_2]$ (Q = PPh_4 (**2a**) and NEt_4 (**2b**))[22] (bdt = 1,2-benzenedithiolate). Both of the model complexes, **2a** and **2b**, and the enzyme active site have *cis*-dioxobis(dithiolene) coordination.

For molybdenum oxidoreductases, the dithiolene part of the molybdopterin cofactor is also expected to coordinate to a molybdenum ion. Actually, in the case of DMSO reductase, the resonance Raman (Mo(VI) and Mo(IV) state)[23] and variable temperature MCD (M(V) state)[24] studies have implicated the chelating coordination of dithiolene to the molybdenum center.

If the tungsten and the molybdenum active sites have two oxo (or sulfide) and three (at least) thiolate ligands with octahedral coordination, (*cis*-$(M^{VI}O_2)^{2+}$ (M = W nad Mo)) as expected from the EXAFS analysis of several enzymes,[15,16,25,26] one of the thiolate ligands should be placed to be *trans* to M^{VI}=O. Thereby strongly donating thiolato ligands have been proposed to labilize the *trans* to M^{VI}=O bonding.[42] If oxo activation is involved in enzyme-substrate reactions (either for M^{VI}=O bond cleavage or for proton transfer to oxygen), the location of thiolate ligands must be crucial for activating the metal–oxo bond.[26]

Based on the tungsten enzyme studies, a variety of models of tungsten enzymes have been prepared and reported. In 1981, Rice et al.[27] compared the electrochemical properties of tungsten complexes with molybdenum analogs, and reported the more negative reduction potentials of oxotungsten complexes, such as, $W^{V}OCl_3L$ (L = α,α′-bipyridyl and *o*-phenanthroline), $W^{V}OClL'_2$, $W^{VI}O_2L'_2$ (L′ = 8-hydroxyquinoline and 8-mercaptoquinoline), which has oxygen, nitrogen and sulfur ligand atoms. An tetra(thiophenolato)monooxotungstate(V) complex, $[W^{V}O(SPh)_4]^-$, was synthesized by Wedd et al.[28,29] as an analog of the molybdenum one. Holm et al.[30,31] examined the oxo transfer capability of various oxotungsten compounds, $W^{VI}O_2(pipdtc)_2$, $W^{VI}O_2(ssp)$, and $W^{VI}O_2(sap)$ (pipdtc = *N*-piperidinecarbondithionate, ssp = 2-(salicylideneamino)benzenethiolate, sap = 2-(salicylideneamino)phenolate). The catalytic oxidation of benzoin by NO_3^- has recently been reported by Cervilla et al.[32] They have used $(NH_4)_2[W^{VI}O_2\{O_2CC(S)Ph_2\}_2]$ as catalyst for the oxidation. The structure and reactivity of terminal sulfide-containing W(VI) species, e.g., $\{HB(Me_2pz)_3\}WS_2(OPh)$ ($HB(Me_2pz)_3$ = hydrotris(3,5-dimethylpyrazol-1-yl)borate) were recently reported by Eagle et al.[33] Also recently dithiolene tungsten(IV and VI) models were synthesized with

1,2-dicyanoethylene-1,2-dithiolate by Sarker et al.[34]

In 1992, we reported the synthesis, structure and reactivities of dioxotungsten(VI), monooxotungsten(V) and (IV) complexes having *two* dithiolene like ligands, bdt.[22] In dioxotungsten(VI) compounds, two thiolato ligands are positioned *trans* to the oxo. This type of complex is thought to be unstable due to *trans* influence between thiolato and oxo ligands.[26] As a model of pterin dithiolene cofactor, we have employed 1,2-benezenedithiolato (= bdt) ligand, since it has a similar dithiolene skeleton with the π-conjugation. In the crystal structure of dioxotungsten(VI) compounds, $(PPh_4)_2[W^{VI}O_2(bdt)_2]$ (**2a**), elongated W^{VI}–S (*trans* to oxo) bonds were observed (ΔW^{VI}–S((*trans* to oxo) − (*cis* to oxo)) = 0.172 Å). The W–S bond elongation by the *trans* influence of oxo ligands is expected to be observed in the tungsten enzyme active site, although the reports of crystallography and EXAFS spectroscopy could not reveal the elongation. In our model complexes, **2a** and **2b**, it has not been clearly understood what stabilizes the mutual *trans* influence between oxo and thiolate due to the uncertainty of the structural dimensions which comes from the weak intensity of high angle reflections in the crystallography.[22] In our continued study, we have obtained fine structural parameters for the 2,3-naphthalenedithiolato complex, $(NEt_4)_2[W^{VI}O_2(ndt)_2]\cdot H_2O$ (**1**). Based on the structural dimensions, we have performed molecular orbital analysis in order to elucidate what stabilizes the mutual *trans* influence between oxo and thiolate. Finally we have revealed the electron delocalization effect for weakening of the *trans* influence by the π-conjugated system involving the dithiolene skeleton and the aromatic ring.

Experimental

All operations were carried out under argon atmosphere. *N*,*N*-Dimethylformamide (DMF), diethyl ether, 1,2-dimethoxyethane (DME), acetonitrile, cyclohexane, and *N*,*N*,*N*′,*N*′-tetramethylethylenediamine (TMEDA) were purified by distillation before use.

2,3-Naphthalenedithiol (ndt-H_2). The titled compound was prepared by a modified method reported for the synthesis of ortho-substituted thiophenol.[35] To 70 mL of cyclohexane was added 2-naphthalenethiol (2.2 g, 14 mmol) and *N*,*N*,*N*′,*N*′-tetramethylene diamine (30 mL, 38 mmol) at 0°C, and an *n*-hexane solution (1.6 M) of *n*-butyllithium (41 mL, 38 mmol) subsequently. The reaction mixture was stirred for 24 h and elemental sulfur (0.88 g, 27 mmol) was added to the well-stirred suspension of the dianion at 0°C. Then the yellow suspension was stirred for an additional 48 h. The cyclohexane was removed in vacuo and replaced by an equal volume of THF. After the THF solution was cooled, $LiAlH_4$ (0.52 g, 13.7 mmol) was added slowly, and the solution was refluxed for 7 h. After cooling to room temperature, the solution was acidified with 100 mL of a 10% HCl aqueous solution at 0°C. The acidic solution was extracted with diethyl ether (2×100 mL) and then the combined organic phase was washed with 10 % HCl aqueous solution (3×50 mL) and with an NaCl-saturated aqueous solution (50 mL), successively. The solution was dried over anhydrous magnesium sulfate and concentrated under reduced pressure to give white powder which was recrystallized from diethyl ether. ^{1}H NMR ($CDCl_3$) δ = 3.38 (s, 2H), 7.41 (q, 2H, J = 3.03, 6.27 Hz), 7.67 (q, 2H, J = 3.03, 6.27 Hz), 7.90 (s, 2H).

Syntheses of $(PPh_4)[W^VO(ndt)_2]$ (3a) and $(NEt_4)[W^VO(ndt)_2]$ (3b). These complexes were synthesized by a modified version of the reported procedure.[22] To a suspension of $(PPh_4)[W^VO(SPh)_4]$[23] (374 mg, 0.383 mmol) in DME–diethyl ether (=1 : 1, v/v) (100 mL) was added ndt-H_2 (147 mg, 0.512 mmol) at room temperature. The mixture was stirred for 4 d. The dark green powder product was collected with filtration and washed with diethyl ether (20 mL). Then, the obtained powder was dried in vacuum and recrystallized from acetonitrile–diethyl ether–*n*-hexane. Yield, 100 mg (26%). Found: C, 58.77; H, 4.13%. Calcd for $C_{48}H_{40}OPWS_4$: C, 59.07; H, 4.13. $C_{47}H_{39}ONWS_4$: C, 50.34; H, 6.34; N, 3.26%. Found: C, 49.88; H, 6.08; N, 3.22%. ν(W=O)=940 cm^{-1}, ν(W–S)=345 cm^{-1} (Raman band). The same procedure was used for the synthesis of **3b**.

Syntheses of $(NEt_4)_2[W^{IV}O(ndt)_2]$ (5). To a stirring acetonitrile solution (100mL) of **3b** (50 mg, 70 mmol) was added NEt_4BH_4 (51 mg, 350 mmol). The blue solution changed to orange immediately and was kept at −20 °C for 1 week. Brown red needle crystals formed were collected by filtration, washed with diethyl ether and dried under vacuum. Yield, 10 mg (17%). Found: C, 49.88; H, 6.08; N, 3.22%. Calcd for $C_{36}H_{52}ON_2WS_4$: C, 51.42; H, 6.23; N, 3.33%. ^{1}H NMR (DMF-d_7) δ = 1.30 (t, 24 H), 3.40 (q, 16H), 7.17 (q, 4H, J = 6.13, 3.21 Hz), 7.65 (q, 4H, J = 6.23, 3.39 Hz), 8.21 (s, 4H). $E_{1/2}$ = −0.58 V (vs. SCE).

Syntheses of $(NEt_4)_2[W^{VI}O_2(ndt)_2]\cdot H_2O$ (1). By the above procedure, a CH_3CN solution (100 mL) of **5** was prepared in situ from **3b** (50 mg, 70 mmol) and NEt_4BH_4 (51 mg, 350 mmol). After the CH_3CN was removed in vacuo, the resultant was washed with CH_3OH, and dried under vacuum. Then to the obtained crude product of **5** were added DMF (4 mL) and Me_3NO (10 mg, 133 mmol). To this solution, diethyl ether (5 mL) vapor was diffused slowly during a period of 1 month in a crystallization apparatus. Orange plate crystals which formed were collected by filtration, washed with diethylether and dried under vacuum. Yield, 10 mg (17%). Found: C, 49.58; H, 6.26; N, 3.31%. Calcd for $C_{36}H_{54}O_3N_2WS_4$: C, 49.42; H, 6.22; N, 3.20%. The water in the crystal came from hydrate in the Me_3NO crystals. ^{1}H NMR (DMF-d_7) δ = 1.34 (tt, 24H), 3.45 (q, 16H), 7.05 (q, 4H, J = 6.23, 3.12 Hz), 7.43 (q, 4H, J = 6.14, 3.21 Hz), 7.49 (s, 4H). E_a = −1.41, E_c = +0.21 V (vs. SCE).

Physical Measurements. Visible spectra were taken on a JASCO Ubest-30 using 1 mM DMF solutions (M = mol dm^{-3}) in a sealed 1 mm-cell. ESR spectra were recorded on a JEOL JES-RE2X spectrometer at 113 and 298 K with a 1 mM acetonitrile–DMF (2 : 1) solution sealed in 5 and 1 mm- quartz tubes under vacuum. IR spectra were recorded on a JASCO FT/IR-3 spectrometer with the use of KBr disk. Raman spectra were taken on a JASCO R-800, NR-1800, and RFT-200 spectrophotometers equipped with HTV-R649 photomultiplier, liq N_2 cooled CCD detector and liq N_2 cooled InGaAs detector, respectively, at 298 K. Exciting radiation was provided by Ar^+ ion (514.5 nm), He–Ne (632.8 nm), or Nd : YAG laser (1064 nm). Wavenumbers of the Raman bands, ν(W=O) and ν(W–S) are determined from the expanded spectra at each region (conditions: 100—50 mW laser power (not focused on the sample), 5 cm^{-1} slit width, 1—5-s dwell time/1.0-cm^{-1} step, 8—64 scans), and calibrations were carried out with natural emissions of a neon lamp from 0—2000 cm^{-1} as standard. Electrochemical measurements were carried out by a Yanaco P-1100 polarographic analyzer with a three-electrode, a platinum wire counter electrode, a saturated calomel electrode, and a saturated calomel electrode separated by glass frits. Redox potentials (E_p) were estimated as the average of E_{pa} and E_{pc} obtained by cyclic voltammograms and differential pulse polarograms. The scan rate was 100 m V s^{-1}. 0.1

M (n-Bu)$_4$NClO$_4$ was used as supporting electrode.

Crystallographic Data Collections and Data Reduction of 1. Orange crystals of **1** was mounted in a glass capillary under argon atmosphere. All measurements were made on a Rigaku AFC-5R diffractometer with graphite monochromated Mo $K\alpha$ radiation and a 12 kW rotating anode generator. Cell constants and an orientation matrix for data collection, obtained from a least square refinement using the setting angle of 25 carefully centered reflections in the range $29.8° < 2\theta < 30.0°$ corresponded to a monoclinic cell with dimensions listed in Table 1. Based on the systematic absences, the successful solutions, and refinement of the structures, the space group were determined to be $P2_1/n$. The data were collected at 23 °C using the ω scan technique to a maximum 2θ value of 55.1°. Of the 12103 reflections which were collected 11311 were unique. The intensities of three representative reflections, measured after every 100 reflections, were shown without any significant change. The linear absorption coefficient for Mo $K\alpha$ is 34.1 cm^{-1}. An empirical absorption correction, based on azimuthal scans of three reflections, was applied, which resulted in transmission factors ranging from 0.84 to 1.00. The data were corrected for Lorentz and polarization effects.

Structure Solution of 1 and the Refinement. The structure was solved by the direct method. The non-hydrogen atoms were refined anisotropically. Hydrogen atom coordinates were included at idealized positions with an assumed C–H distance of 1.08 Å and the hydrogen atoms were given with the same temperature factor as that of carbon atom to which they were bonded. The final cycles of least-squares refinement were based on 8863 observed reflections ($I > 3.00\sigma(I)$), and 460 variable parameters and converged with $R = 0.023$ and $R_w = 0.033$.

Neutral atom scattering factors were taken from Ref. 37. Anomalous dispersion effects were included in F_{calcd}; the values for $\Delta f'$ and $\Delta f''$ were taken from Ref. 37. All calculations were performed using the TEXSAN crystallographic software package of Molecular Structure Corporation.

Molecular Orbital Calculations. Molecular orbital calculations of the extended Hückel type were carried out using the CAChe software package (CAChe Scientific Inc., 1993). The parameters for W (Ref. 37) and S (Ref. 38) were taken from the reported work, while those of C and H are standard ones. The bond order calculation was performed for the crystal structure of the tungsten(VI)–naphthalenedithiolato structure, **1**. To evaluate the bonding nature of W^{VI}–S bonds, the calculation was also done for the idealized octahedral model of $[W^{VI}O_2(SH)_4]^{2-}$ (Fig. 8). The coordination geometry of W atom were assumed with a C_2 symmetry for the simple model complex, $[W^{VI}O_2(SH)_4]^{2-}$. The W^{VI}=O, W^{VI}–S (*trans* to W^{VI}=O, and *cis* to W^{VI}=O). The S–H bond distances used are 1.7470 Å, 2.5944 Å for **9** and 2.4230 Å for **10**, 2.423 Å, and 1.3400 Å, respectively. The W^{VI}–S–H angle used is 109.47°.

Table 1. Crystal and Refinement Data for $(NEt_4)_2[W^{VI}O_2(ndt)_2]\cdot H_2O$ (**1**)

	1
Chemical formula	$C_{36}H_{54}O_3N_2S_4W$
MW	874.92
Cryst.color	Red-orange
Cryst.shape	Plate
Cryst.syst.	Monoclinic
Space group	$P2_1/n$ (No. 14)
a/Å	7.396(2)
b/Å	17.581(2)
c/Å	28.839(2)
β/deg	95.35(2)
V/Å^3	3734(3)
Z	4
d_{calcd}/g cm^{-3}	1.556
Radiation	Mo $K\alpha$
μ(Mo $K\alpha$)/cm^{-1}	34.10
F(000)	1784
Temp/°C	23
Scan speed/deg min^{-1}	8
2θrange/deg	6—55
Octants	$+h, +k, \pm l$
Measured reflections	12103
Unique reflections	11311 (R_{int}=0.034)
Observed reflections ($I_0 > 3\sigma(I)$)	8863
R[a)]	0.023
R_w[b)]	0.030
Goodness of fit	1.25

a) $R=(\Sigma||F_o|-|F_c||)/\Sigma|F_o|$. b) $R_w=(\Sigma w||F_o|-|F_c||^2)/\Sigma wF_o^2)^{1/2}$.

Results

Synthetic Studies. We have synthesized $(W^{VI}O_2)^{2+}$ and $(Mo^{VI}O_2)^{2+}$ bis(dithiolato) complexes (dithiolato = ndt, bdt and its derivatives, and 1,2-dicyanoethylene-1,2-dithiolato ($S_2C_2(CN)_2$)) by the three-step method via O-atom transfer reaction and ligand exchange reaction as shown in Fig. 1.

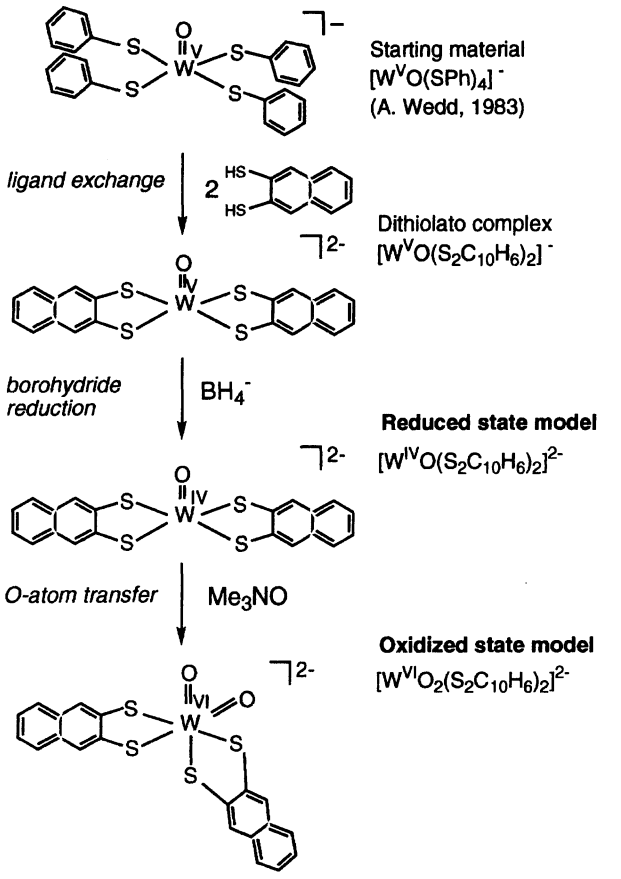

Fig. 1. The synthesis of $(NEt_4)_2[W^{VI}O_2(ndt)_2]\cdot H_2O$ (**1**), complex.

In the past, there were some reports of procedures employing one-pot synthesis to obtain dioxotungsten(VI) and dioxomolybdenum(VI) complexes from $(M^{VI}O_2)^{2+}$ complexes, such as, $[M^{VI}O_2(acac)_2]$ (acac = acetylacetonate).[26,27,30,39] An attempt to synthesize the $(Mo^{VI}O_2)^{2+}$ complex with three or four thiolate ligands was reported without success.[26,39] An important conclusion of these reports[26,39] was that this type of complex was considered not to be isolated due to the strong *trans* influence by a Mo^{VI}=O group towards one of the thiolate ligands. For example,[40] oxo-eliminated complex, tris(1,2-styrenedithiolato)molybdenum(VI), resulted from the ligand exchange reaction of $[Mo^{VI}O_2(acac)_2]$ with disodium-1,2-styrenedithiolate, although the ratio of the ligand and the molybdenum complex was not described in the report.

To avoid the oxo-elimination reaction, we have employed the low solubility of the bis(dithiolato)monooxotungsten(V) complex in the ligand exchange reaction at the first step.[22] For example, in the case of naphthalenedithiolato complex, **1**, we have first synthesized the $(W^{V}O)^{3+}$ complex, **3b**, by the ligand exchange reaction of $(NEt_4)[W^{V}O(SPh)_4]$[29] with two equivalents of ndt-H_2. The reduction of this $(W^{V}O)^{3+}$ complex, **3b**, with borohydride anion gave $(W^{IV}O)^{2+}$ complex, **5**. The $(W^{VI}O_2)^{2+}$ complex, **1**, was obtained from O-atom transfer reaction between **5** and Me_3NO.

Another advantage of our method is to employ the O-atom transfer reaction at the final step to produce the $(W^{VI}O_2)^{2+}$ and $(Mo^{VI}O_2)^{2+}$ complexes. Utilizing this reaction, we can examine the stability of the target complex by the vibrational and UV/vis spectra. For example,[41,42] the $(Mo^{VI}O_2)^{2+}$ complex, $[Mo^{VI}O_2\{S_2C_2(CN)_2\}_2]^{2-}$ (**8**) ($S_2C_2(CN)_2$ = 1,2-dicyanoethylene-1,2-dithiolato) was isolated in the reaction between Me_3NO and $[Mo^{IV}O\{S_2C_2(CN)_2\}_2]^{2-}$. On the contrary, in the case of the reaction of $[Mo^{IV}O\{S_2C_2(COOMe)_2\}_2]^{2-}$, the formation of $[Mo^{VI}O\{S_2C_2(COOMe)_2\}_2]^{2-}$ was only observed transiently in the various spectra (UV/vis, Raman and ^{1}H NMR). This study has revealed the stability of $(Mo^{VI}O_2)^{2+}$ dithiolene complexes where the electron withdrawing effect by the substituent on the dithiolene ligand can modulate the ease for the oxidation of dithiolene ligand. Thus, by the O-atom transfer method, in our case, $(W^{VI}O_2)^{2+}$ and $(Mo^{VI}O_2)^{2+}$ thiolato complexes were synthesized successfully without the oxo-elimination or the thiolate oxidation.[22,43]

Crystal Structure of $(NEt_4)_2[W^{VI}O_2(ndt)_2]\cdot H_2O$ (1). Figure 2 shows the ORTEP drawing of the anion part of $(NEt_4)_2[W^{VI}O_2(ndt)_2]\cdot H_2O$ (**1**). In Tables 1 and 2, crystal and refinement data, and the final atomic positional parameters with standard deviations were listed. Figure 3 and Table 3 show the selected bond angles and bond lengths for **1**. In this structure, no disorder problem associated with Et_4N^+ cations was not observed. Both the cations, the complex anion, and the H_2O molecule are well separated from each other. The W(VI) ion has octahedral coordination with two naphthalenedithiolate (ndt) and *cis*-dioxo ligands. Such dioxotungsten(VI) and dioxomolybdenum(VI) complexes are quite rare, as mentioned above. The structure of $(Mo^{VI}O_2)^{2+}$ (M = W and Mo) dithiolate complexes, **2a**,

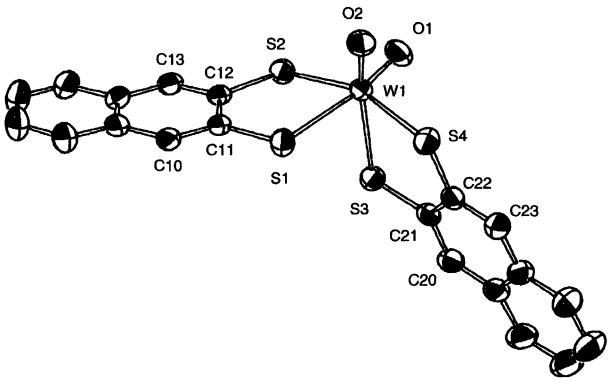

Fig. 2. The ORTEP drawing of anion part of $(NEt_4)_2[W^{VI}O_2(ndt)_2]\cdot H_2O$ (**1**). The 50% probability ellipsoids are shown.

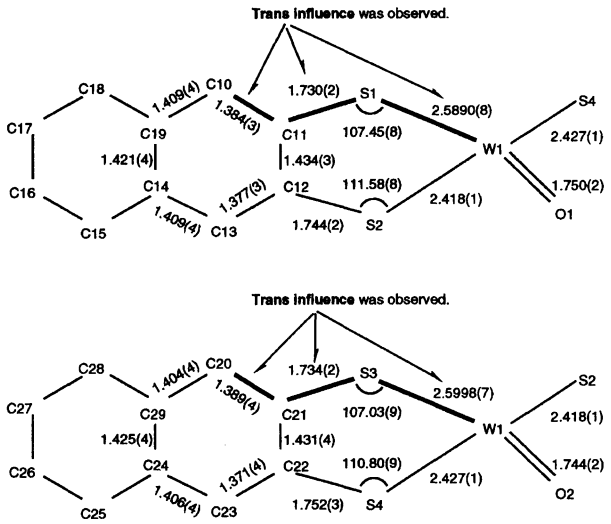

Fig. 3. Selected bond angles (deg.) and bond lengths (Å) in the structure of $(NEt_4)_2[W^{VI}O_2(ndt)_2]\cdot H_2O$ (**1**).

$(PPh_4)_2[Mo^{VI}O_2(bdt)_2]$ (**7**), and **8** has revealed the existence of the two longer M^{VI}–S bonds and the two smaller M^{VI}–S–C bond angles located at the *trans* positions of the two M^{VI}=O groups as the results of mutual *trans* influence between the oxo and the thioalate which have strong σ-and π- donating effects.[22,41–43] The smaller M^{VI}–S–C bond angle has suggested the presence of thioketone-like sulfur ligand atoms which weaken the M^{VI}–S bonds *trans* to the oxo ligands, and the angle contributes to the stabilization of the $(M^{VI}O_2)^{2+}$ thiolato structure, particularly at the *trans* positions. In the case of this naphthalenedithiolato (ndt) complex, **1**, an accurate crystal structure was obtained which provides the detailed structural parameters. Thus it seems possible to infer the reason for the stable $(M^{VI}O_2)^{2+}$ thiolato coordination. A particularly interesting point is the significant structural difference found in the W^{VI}–S–C bond lengths between the *trans* to the two oxo groups and the *cis* to them. These differences are clearly as follows: W^{VI}–S, $\Delta(trans-cis)$ = 0.171 Å; S–C, $\Delta(trans-cis)$ = −0.016 Å. The difference in W^{VI}–S–C angles is also noted: < (W^{VI}–S–C), $\Delta(trans-cis)$ = −3.95°. In addition to these clear differences in the structure, the

Table 2. Fractional Atomic Coordinates and Thermal Parameters for $(NEt_4)_2[W^{VI}O_2(ndt)_2]\cdot H_2O$ (**1**)

Atom	x	y	z	B(eq)
W1	0.47332(1)	0.035351(5)	0.149082(3)	2.604(4)
S1	0.48248(9)	0.18066(4)	0.13491(3)	3.31(3)
S2	0.15950(9)	0.05998(4)	0.12198(2)	3.01(2)
S3	0.37314(9)	0.07049(4)	0.23043(2)	3.01(2)
S4	0.7659(1)	0.05036(4)	0.19371(2)	3.30(3)
O1	0.3954(3)	−0.0574(1)	0.15655(7)	3.73(8)
O2	0.6025(3)	0.0249(1)	0.10187(7)	3.79(9)
C10	0.2475(4)	0.2779(1)	0.08666(8)	2.9(1)
C11	0.2757(3)	0.2065(1)	0.10624(8)	2.46(8)
C12	0.1283(3)	0.1532(1)	0.10223(8)	2.44(8)
C13	−0.0399(3)	0.1745(1)	0.08184(8)	2.8(1)
C14	−0.0681(3)	0.2472(1)	0.06180(8)	3.0(1)
C15	−0.2386(4)	0.2695(2)	0.0391(1)	4.2(1)
C16	−0.2601(5)	0.3390(2)	0.0183(1)	5.3(2)
C17	−0.1156(5)	0.3901(2)	0.0198(1)	5.4(2)
C18	0.0493(5)	0.3716(2)	0.0422(1)	4.4(1)
C19	0.0788(4)	0.2994(1)	0.06369(9)	3.2(1)
C20	0.5544(4)	0.0710(1)	0.31739(9)	3.0(1)
C21	0.5651(3)	0.0657(1)	0.26969(8)	2.62(9)
C22	0.7405(3)	0.0560(1)	0.25341(9)	2.66(9)
C23	0.8929(4)	0.0519(2)	0.2842(1)	3.1(1)
C24	0.8823(4)	0.0562(2)	0.3326(1)	3.2(1)
C25	1.0372(4)	0.0497(2)	0.3656(1)	4.5(1)
C26	1.0212(5)	0.0517(2)	0.4120(1)	5.4(2)
C27	0.8513(5)	0.0603(2)	0.4287(1)	5.0(2)
C28	0.6980(5)	0.0673(2)	0.3986(1)	4.1(1)
C29	0.7088(4)	0.0659(1)	0.34949(9)	3.1(1)
N1	0.9682(3)	0.3075(1)	0.22457(7)	2.57(7)
C111	1.0911(4)	0.3766(1)	0.2276(1)	3.5(1)
C112	1.2416(5)	0.3750(2)	0.1961(1)	5.6(2)
C113	0.8259(4)	0.3223(2)	0.2584(1)	3.4(1)
C114	0.6949(4)	0.2581(2)	0.2637(1)	4.7(1)
C115	0.8807(4)	0.2956(1)	0.17572(9)	3.1(1)
C116	0.7656(5)	0.3611(2)	0.1558(1)	4.7(1)
C117	1.0751(4)	0.2353(1)	0.2372(1)	3.1(1)
C118	1.1691(4)	0.2338(2)	0.2858(1)	4.2(1)
N2	−0.3200(3)	0.3358(1)	0.44003(7)	2.65(8)
C121	−0.2152(4)	0.3384(2)	0.48781(9)	3.2(1)
C122	−0.0952(5)	0.4075(2)	0.4972(1)	4.5(1)
C123	−0.4465(4)	0.4037(2)	0.4328(1)	3.4(1)
C124	−0.5878(5)	0.4097(2)	0.4668(1)	5.3(2)
C125	−0.4253(4)	0.2617(1)	0.4381(1)	3.4(1)
C126	−0.5427(5)	0.2475(2)	0.3931(1)	4.9(2)
C127	−0.1941(4)	0.3398(2)	0.40151(9)	3.3(1)
C128	−0.0553(5)	0.2767(2)	0.4022(1)	5.1(2)
O3	0.9512(3)	0.0985(1)	0.81262(8)	4.8(1)

naphthalene rings have also sightly, but not significantly, longer C–C bonds positioned next to the long W^{VI}–S bonds (C10–C11, 1.384(3); C20–C21, 1.389(4) Å). On the side of short W^{VI}–S bonds, the C–C bonds are 1.377(3) and 1.409(3) Å for C12–C13 and C22–C23. Thus, the detailed structural parameters show the extent of the strong π-donating effect of the oxo and thiolate ligands (mutual *trans* influence) to be spread into the naphthalenedithiolato (ndt) ligand through π-orbitals on the O–W^{VI}–S–C–C structure.

Our theoretical calculation supports the bond elongation and shrinkage at the W^{VI}–S–C–C moiety. Figure 4 shows the calculated bond order[45] for the anion part of **1**. The calculated bond orders of W^{VI}–S (*trans* to W^{VI}=O) are definitely smaller than that of W^{VI}–S (*cis* to W^{VI}–O) with a difference of 0.266 (mean). For the S–C (*trans* to oxo) bonds, 0.050 (mean) larger bond orders were observed than that of the (*cis* to oxo) S–C bond. Smaller (0.032 (mean)) bond orders appeared again for C11–C10 and C21–C20 bond (*trans* to oxo) than the values of C12–C13 and C22–C23 (*cis* to oxo). The bond length difference indicates that the strong π-donating effect of oxo and thiolate ligands is diffused into the π-conjugated bonds of the dithiolene skeleton connected with the naphthalene ring.

Another important result of the calculation is that the

Table 3. Comparison of Structural Parameters (Å, deg) for $(NEt_4)_2[W^{VI}O_2(ndt)_2]\cdot H_2O$ (**1**) and $(PPh_4)_2[W^{VI}O_2(bdt)_2]$ (**2a**)

	1	**2a**
W=O (mean)	1.747(4)	1.730(7)
Range	1.744(2)—1.750(2)	1.727(9)—1.737(6)
W–S		
trans to oxo (mean)	2.5944(76)	2.597(10)
Range	2.5890(8)—2.45998(7)	2.590(3)—2.604(3)
cis to oxo (mean)	2.423(6)	2.425(12)
Range	2.418(1)—2.427(1)	2.416(3)—2.433(3)
S–C		
trans to oxo (mean)	1.732(3)	1.740(4)
Range	1.730(2)—1.734(2)	1.743(9)—1.737(8)
cis to oxo (mean)	1.748(6)	1.751(7)
Range	1.744(2)—1.752(3)	1.746(10)—1.756(9)
∠(W–S–C)		
trans to oxo (mean)	107.24(30)	106.3(2)
Range	107.03(9)—107.45(8)	106.1(3)—106.4(3)
cis to oxo (mean)	111.19(55)	110.4(0)
Range	110.80(9)—111.58(8)	110.4(3)—110.4(4)

a) The number in the parentheses represents the individual standard deviation or the standard deviations from the mean, σ. $\sigma = (\sum_{i=1}^{N}(x_i - x_{mean})^2/N(N-1))^{1/2}$.

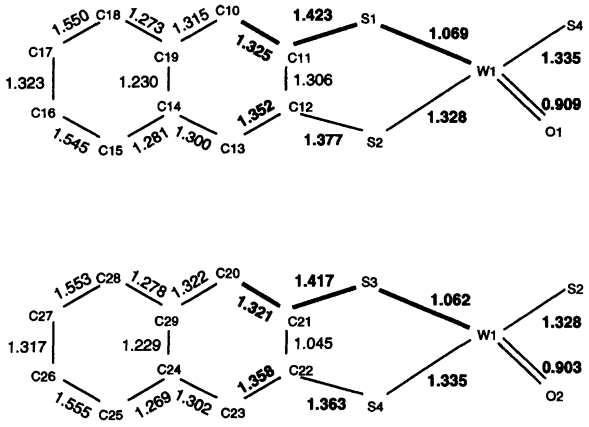

Fig. 4. Obtained bond orders for the structure of $[W^{VI}O_2(ndt)_2]^{2-}$. Anion part structure of **1** was used for extended Hückel calculation.

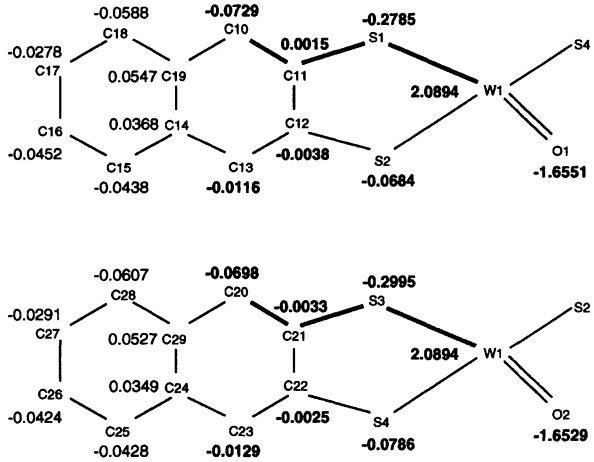

Fig. 5. Obtained atom charges for the structure of $[W^{VI}O_2(ndt)_2]^{2-}$. Anion part structure of **1** was used for extended Hückel calculation.

highly negative charges are accumulated on the sulfur atoms *trans* to oxo ligands. The calculated charges on the sulfur atoms are −0.2890 (mean, *trans* to oxo) and −0.0735 (mean, *cis* to oxo) as shown in Fig. 5. Those negative charges are required to be stabilized by the electron delocalizing device such as π-conjugated ligands which serve as an electron buffer or as acceptor. This is probably a reason why 1,2-benzenedithiolate type ligands, e.g. bdt and ndt, are suitable to synthesize bis(dithiolato)*cis*-dioxotungstate(VI) complexes. For the other $(W^{VI}O_2)^{2+}$ dithiolene complexes **2a**, **7**, and **8**,[22,41—43] the modulation of the mutual *trans* influence can be done by the same electron accepting and delocalizing mechanism.

The Comparison of Electronic Effects between 2,3-Naphthalenedithiolate and 1,2-Benzenedithiolate. From the above discussion, the extended π-conjugation system can contribute to decrease the mutual *trans* influence between oxo and thiolate. In order to examine the effect of π-conjugation extension, we have compared the naphthalenedithiolato (= ndt) and the benzenedithiolato (= bdt) complexes for $(W^{VI}O_2)^{2+}$, $(W^{IV}O)^{2+}$, and $(W^{V}O)^{3+}$ states in terms of their structural and electronic properties.

$(W^{VI}O_2)^{2+}$ Complexes. Structural parameters, UV/vis absorption maxima, Raman (IR) frequencies, and reduction potentials were compared. In the UV/vis spectra, naphthalenedithiolato complex, **1**, shows a quite different pattern which is probably due to the overlap of ligand absorption. Therefore, in this case, we can not compare the lowest energy of absorption maxima associated with the electronic transi-

tion of HOMO (mainly Spπ (*trans* to oxo) orbital)⟶LUMO (mainly Wdπ orbital) which causes W^{VI}=O activation, because the LUMO is antibonding at the W^{VI}=O part.[42]

As shown in Table 3, the unequal W^{VI}=O bond lengths in the naphthalenedithiolato (ndt) complex, **1**, (1.744(2) and 1.750(2)) Å have a mean value, 1.747(4) Å, which is almost the same compared with that of the benzenedithiolato complex, $(PPh_4)_2[W^{VI}O_2(bdt)_2]$ (**2a**) (1.730(7) Å (mean)). For other structural parameters, however, the dithiolato (W^{VI}–S–C) moiety did not shown any significant difference between **1** and **2a**, such as the two long W^{VI}–S bonds *trans* to the two oxo ligands, and the two short W^{VI}–S bonds *cis* to them, the S–C bonds and the ∠ (W^{VI}–S–C) angles.

Cyclic voltammograms of **1** and $(NEt_4)_2[W^{VI}O_2(bdt)_2]$ (**2b**) in DMF solution exhibit irreversible reduction peaks at −1.41 and −1.26 V (vs. SCE), respectively, presumably assignable to the W(VI)/W(V) redox process containing the successive O-atom releasing reactions[46] when scanned in the cathodic direction. The naphthalenedithiolate ligand shifts the reduction potential of $(W^{VI}O_2)^{2+}$ state to the negative side ($\Delta(\mathbf{1}-\mathbf{2b}) = -0.15$ V) compared with that of benzenedithiolate. The ligand, ndt, should be more polarizable than the smaller conjugation, bdt ligand. If a dithiolato ligand has large polarizability, the dithiolato ligand can delocalize a electron on thiolate ligand atom to form a thioketonic sulfur atom. Therefore, the observed shift is ascribed to the elevating of the vacant W 5d energy level by the weaker W–S π-interaction by the thioketonic ligand contributes to the stabilization of O=W^{VI} bond. Therefore, the electron withdrawing ligand, naphthalenedithiolate, stabilizes the W^{VI}=O bond through the weakening of the W^{VI}–S (*trans* to oxo) bond, although the bond weakening is not detected.

The Raman spectra of **1** (Fig. 6) and **2b** show two intense bands at ca. 880 and ca. 840 cm^{-1} assignable to symmetric (ν_s) and asymmetric (ν_{as}) W^{VI}=O stretchings, respectively. The values of these bands indicate the activation of oxo-tungsten bonds by the *trans* influence of thiolate coordination.[42] Relatively weak bands were observed between 300 to 200 cm^{-1}. The bands at 368, 358, and 339, and 370, 352, and 326 cm^{-1} for **1** and **2b**, respectively, are associated with the W^{VI}–S stretchings. The assignment is from the excitation profiles of **2b** (457.9—514.5 and 632.8 nm excitation) as reported before.[42] In the profile, the band of **2b** at 370 cm^{-1} showed a highly enhanced intensity at the shorter wavelength. Due to the complexity of the spectrum of **1** in the region of 200—300 nm, we could not compare the $\nu(W^{VI}$–S) bands of **1** and **2b**. The complexity of this region arises from the overlapping of the naphthalene ring bands.

The elongated (*trans* to oxo) and the standard (*cis* to oxo) W^{VI}–S(thiolate) bonds exist in the crystal structure of **1** and **2a**. Then two kinds of $\nu(W^{VI}$–S) bands are expected in the spectra. Subramanian et al.[47] have reported the estimation of a lower frequency shift (at ca. 250 cm^{-1}) for the elongated Mo^{VI}–S(thioether) bond with use of the Budger's rule.[48] In our case, the existence of another $\nu(W^{VI}$–S) band can be expected in a lower frequency region (below 300 cm^{-1}),

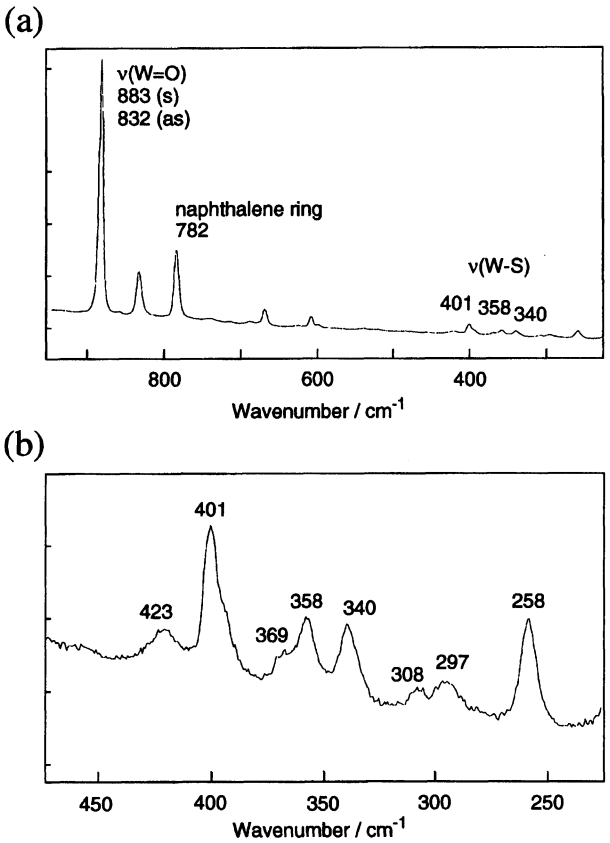

Fig. 6. Raman spectrum of $(NEt_4)_2[W^{VI}O_2(ndt)_2]\cdot H_2O$ (**1**) in solid state. A single crystal was used. (632.8 nm excitation.)

although the shifted bands have not yet to be determined precisely.

$(W^{IV}O)^{2+}$ Complexes. The electronic properties of the (naphthalenedithiolato)monooxotungstate(IV) complex was compared with those of the benzenedithiolato complex in terms of redox potential, $\nu(W^{IV}$–S) and $\nu(W^{IV}$=O) band, and UV/vis absorption maxima (Table 4 and Fig. 7). The naphthalenedithiolato complex, **5**, exhibits quasi-reversible redox couple at −0.52 V (vs. SCE). This is assignable to the W(IV)/W(V) couple. A comparison of $E_{1/2}$ values between two types of complexes, **5** and $(NEt_4)_2[W^{IV}O(bdt)_2]$ (**6**), shows a positive shift ($\Delta(\mathbf{5}-\mathbf{6}) = -0.11$ V). The observed shift is ascribed to elevation of the occupied W 5d energy level due to the extension of the π-conjugated system.

The above rationale predicts red shifts of the LMCT bands of naphthalenedithiolato complex, **5**, compared with the case of benzenedithiolato complex, **6**. For **5**, as shown in Fig. 7, two strong and two weak absorption bands are observed at 363 and 379, and 399 and 423 nm, respectively. The strongest absorption in the range 363—379 nm is probably assignable to the π–π* transition of the naphthalenedithiolato ligand. Because of the complexity of the UV/vis spectra due to overlap of ligand absorptions, the shift of LMCT band (S⟶W) between **5** and **6** can not be estimated correctly.

In the Raman spectra of two $(W^{IV}O)^{2+}$ complexes, **5** and **6**, the bands at 920 and 369 cm^{-1}, and 904 and 370 cm^{-1} were observed, respectively. These bands are associated with

Table 4. Raman (IR) bands of ν(W=O) and ν(W–S), UV/vis Absorption Maxima, and Redox Potential of $(NEt_4)_2$ $[W^{VI}O_2(ndt)_2]\cdot H_2O$ (**1**), $(NEt_4)_2[W^{VI}O_2(bdt)_2]$ (**2b**), $(NEt_4)_2$ $[W^{IV}O(ndt)_2]$ (**5**), and $(NEt_4)_2$ $[W^{IV}O(bdt)_2]$ (**6**)

	Raman (IR) band solid state cm^{-1}		UV/vis absorption in DMF nm (M^{-1} cm^{-1})	Redox potential in DMF (V vs. SCE)
	ν(W=O)	ν(W–S)	$\lambda_{max}(\varepsilon)$	
1	883 (884) (ν_s)	368	391 (sh, 20000)	−1.41
	832 (835) (ν_{as})	357	437[a] (sh, 10000)	+0.21
		339	475[a] (sh, 3700)	(Irreversible)
2b	885 (888) (ν_s)	370	323 (sh, 15000)	−1.26
	843 (847) (ν_{as})	352	419 (2300)	+0.14
		326	483 (1300)	(Irreversible)
5	920	369	363 (sh, 17000)	−0.52
			379 (26000)	
			419 (sh, 2400)	
			526 (1300)	
6	904 (906)	370	325 (9200)	−0.63
			399 (1100)	
			423 (sh, 570)	

a) The peaks of absorption bands were determined by the fourth derivatives of the spectrum.

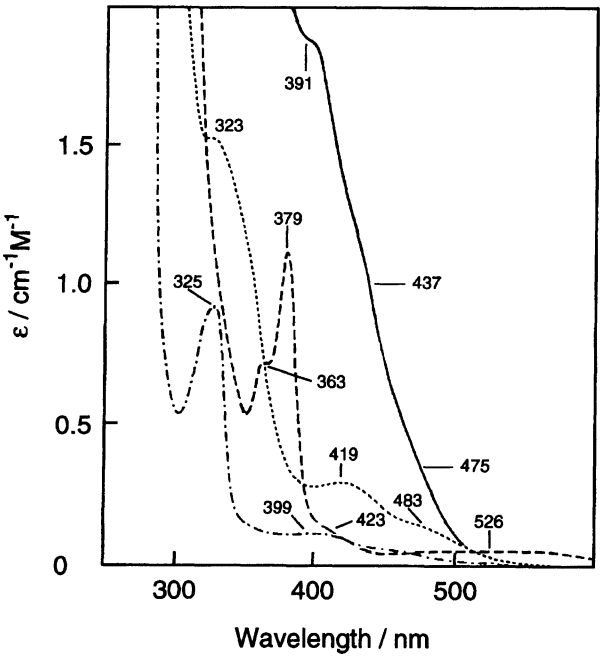

Fig. 7. UV/vis spectra of $(NEt_4)_2[W^{IV}O(ndt)_2]$ (**5**) (---), $(NEt_4)_2[W^{IV}O(bdt)_2]$ (**6**) (-·-), $(NEt_4)_2[W^{VI}$-$O_2(ndt)_2]\cdot H_2O$ (**1**) (—), and $(NEt_4)_2[W^{VI}O_2(bdt)_2]$ (**2b**) (– – –) in DMF.

the vibrations of W^{IV}=O and W^{IV}–S bonds, respectively. The trend of the difference in $\nu(W^{IV}=O)$ band wavenumber between **5** and **6** (Δ(**5** − **6**) = +16 cm^{-1}) is consistent with the weaker π-donating nature of naphthalenedithiolato ligand as observed in the redox potential. Considering the competitive π-donation between oxo and thiolato to the metal vacant d-orbital, the W^{IV}=O bond strengthening (large W=O π-overlap is clearly expected when the W^{IV}–S π-overlap is decreased

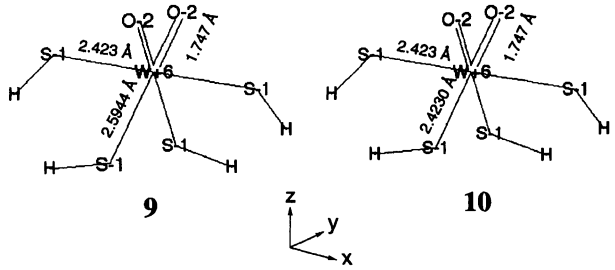

Fig. 8. Calculated structure of long and short S–H (*trans* to oxo) bond models, $[W^{VI}O_2(SH)_4]^{2-}$ (**9** and **10**).

in the case of the weaker π-donating naphthalenedithiolate.

$(W^VO)^{3+}$ Complexes. ESR spectra at X-band frequencies of the naphthalenedithiolato complex, **3a**, exhibits rhombic symmetry signals. Table 5 lists the obtained g and A values compared with the benzenedithiolato complex, (PPh_4)-$[W^VO(bdt)_2]$ (**4**).[49] For each signal, there are two hyperfine lines due to ^{183}W (14.40 atom %; $I = 1/2$).

From the values of hyperfine splitting in solution (A_{iso}), we can compare the electronic effect of ligands. Because the A_{iso}

Table 5. ESR Parameters for $(PPh_4)[W^VO(ndt)_2]$ (**3a**) and $(PPh_4)[W^VO(bdt)_2]$ (**4**) Complexes

Parameters	**3a**	**4**
g_{iso}	1.961	1.960
A_{iso} (mT)	5.6	5.8
$g1$	2.054	2.044
$g2$	1.930	1.931
$g3$	1.910	1.911
$A1$ (mT)	8.0	8.2
$A2$ (mT)	4.44	4.16
$A3$ (mT)	4.6	4.4

value is dominated by the Fermi contact interaction, larger A_{iso} value indicates higher electron density on the W atom which was influenced by the donating ability of the ligand. In the case of the 2,3-naphthalenedithiolato complex, **3a**, A_{iso} is 5.6 mT, which is sightly smaller than that of 1,2-benzenedithiolato complex, **4** (5.8 mT). Therefore, from the ESR parameter, naphthalenedithiolate ligand is considered as a weaker electron donating ligand than benzenedithiolato ligand in the $(W^{V}O)^{3+}$ state.

Discussion

Theoretical Analysis for the Elongated W–S (*Trans* to Oxo) Bond as Observed in *cis*-$(W^{VI}O_2)^{2+}$ Thiolato Complexes, 1 and 2a. To clarify what makes the elongated W^{VI}–S bond (*trans* to W^{VI}=O), we have performed extended Hückel calculations for the two model complexes $[W^{VI}O_2(SH)_4]^{2-}$ with the long W^{VI}–S bond (2.5944 Å for **9**) and the short W^{VI}–S bond (2.4230 Å for **10**) at the *trans* position to W^{VI}=O as shown in Fig. 8. The first molecule, **9**, is a model for the elongated W^{VI}–S bond length (2.5944 Å) as observed in the crystal structure of **1**. The second model, **10**, represents a normal W^{VI}–S bond length which is fixed to the W^{VI}–S (*cis* to oxo) length (2.4230 Å). Table 6 summarizes the calculated overlap populations of W^{VI}=O and W^{VI}–S (both *trans* and *cis* to oxo), ($P(W^{VI}=O)$ and P(W–S), respectively), their σ and π bond components[50] (P_σ and P_π) and charges on each ligand atom (Q). For Ta^{V}=S bond, Tatsumi et al.[51] have reported the sulfur-to-tantalum π-donor interactions with extended Hückel calculations. They have explained the decrease in π-interaction between Ta(V) and S as due to the strong π-donor capability (*trans* influence) of the cyclopentadienyl ligand.

When the W^{VI}–S (*trans* to oxo) bond length is elongated from 2.4230 Å (in **9**) to 2.5944 Å (in **10**), the P(W=O) becomes larger (ΔP(W=O)=+0.032). The difference (Δ(**9**–**10**)) in σ-bond component, ΔP_σ(W=O), is −0.020 (decrease) and in the π-component, ΔP_π(W=O), is +0.052 (increase). Particularly the Wd_π–Op_π interaction mainly contributes to the value of ΔP_π(W=O)($\Delta P_\pi(Wd_\pi–Op_\pi)$= +0.048). For the W=O bond, an increase in covalency is expected from an increase in Wd_π–Op_π interactions when the W^{VI}–S (*trans* to oxo) bond length is elongated.

In the case of W^{VI}–S(*cis* to oxo) bond, the overlap population, P(W–S (*cis* to oxo)), is also increased (ΔP(W–S (*cis* to oxo))= +0.403) by the elongation of W–S (*trans* to oxo) bonds. As shown in Table 6, the increase in the covalency of W–S (*cis* to oxo) bond will result mainly in π interactions (ΔP_π = +0.291), if the W–S (*trans* to oxo) bond is elongated.

Different from the above two cases, a decrease in overlap populations (P) was observed for W^{VI}–S (*trans* to oxo) bonds ($\Delta P(W^{VI}$–S (*trans* to oxo))= −0.108), when the W^{VI}–S (*trans* to oxo) bonds were elongated. The σ-component (ΔP_σ) of ΔP(W–S (*trans* to oxo)) is −0.042 (decrease). The π component (ΔP_π) of ΔP(W–S (*trans* to oxo)) is −0.065 (decrease) where the lowering of the Wd_π–Sp_π, d_π interaction mainly contributes to the decrease in P_π components ($\Delta P_\pi(Wd_\pi–Sp_\pi, d_\pi)$= −0.068 (decrease)). For W^{VI}–S (*trans* to oxo) bonds, the Wd_π–Sp_π and Wd_π–Sd_π interactions are decreased when the W^{VI}–S (*trans* to oxo) bond is elongated.

As observed in the calculation of **1**, the negative charges are accumulated on the sulfur atoms (*trans* to oxo) for **9** (−0.492) and **10** (−0.482). Therefore, some electron delo-

Table 6. Overlap Populations (P) and Their σ, π Components (P_σ and P_π) on Each Bonds, W^{VI}=O, W^{VI}–S (*trans* to oxo), and W^{VI}–S (*cis* to oxo), and Net Atomic Charges (Q) on Each Atoms for two Model Complexes, $[W^{VI}O_2(SH)_4]^{2-}$ (**9** and **10**)
$P_\pi(Wd_\pi–Op_\pi)$, $P_\pi(Wd_\pi–Sd_\pi)$, and $P_\pi(Wd_\pi–Sp_\pi)$,[50] are the contribution of Wd_π–Op_π, Wd_π–Sp_π, and Wd_π–Sd_π interactions to P_π, P_π, and P_π values, respectively.

		W–S (*trans* to oxo) bond length		
		2.5944 Å(**9**)	2.4230 Å(**10**)	ΔP(**9**–**10**)
W^{VI}=O	P	0.226	0.194	+0.032
	P_σ	0.067	0.087	
	P_π	0.159	0.107	+0.052
	$P_\pi(Wd_\pi–Op_\pi)$	0.147	0.099	+0.048
Net charge of O	Q	−1.666	−1.682	
W^{VI}–S	P	0.572	0.680	
(*trans* to oxo)	P_σ	0.392	0.434	
	P_π	0.180	0.245	
	$P_\pi(Wd_\pi–Sp_\pi)+P_\pi(Wd_\pi–Sd_\pi)$	0.157	0.225	
Net charge of S	Q	−0.492	−0.482	
W^{VI}–S	P	0.736	0.333	+0.403
(*cis* to oxo)	P_σ	0.476	0.365	+0.111
	P_π	0.259	−0.324	+0.583
	$P_\pi(Wd_\pi–Sp_\pi)+P_\pi(Wd_\pi–Sd_\pi)$	0.234	−0.052	+0.286
Net charge of S	Q	+0.143	+0.196	

calizing π systems are needed to diffuse the negative charge which is produced by weakening of the Mo–S (*trans* to oxo) π-bonding.

Our theoretical analysis indicates that the elongation of the W^{VI}–S (*trans* to oxo) bonds is primarily produced by the increasing of the ligand-metal π bonding in W^{VI}=O and W^{VI}–S (*cis* to oxo) and the *trans* influence results in the accumulation of negative charges on the sulfur atoms *trans* to oxo.

The Structure of Tungstopterin Cofactor: From the View Point of Model Complexes. The structure of the aldehyde ferredoxin oxidoreductase has been reported by Chan et al.[21] Surprisingly, the reported structure of tungstopterin cofactor closely resembles our model complexes, **1** and **2a**.[53] Both of the enzyme active site and the model complexes (**1** and **2a**) have *cis*-dioxobis(dithiolene) coordination on a hexacoordinated tungsten atom. Because of the uncertainty of the oxo ligands and its geometry on the tungsten ion of the enzyme, we can not decide whether the precise geometry of the tungsten ion is an octahedron, a bicapped tetrahedron or a trigonal prism. The existence of two oxo ligands and the oxidation state of tungsten ion in the enzyme is not conclusive crystallographically but is supported by the EXAFS analysis.[15] Only the coordination structure of thiolates at the W ion can be compared with the model complexes, **1** and **2a**. For example, the angle (ca. 97°) between the planes of the dithiolene ligands for the tungstopterin cofactor can be compared with that (89°) for the model complex, **2a**. Unfortunately, the other structural parameters of the tungstopterin cofactor, e.g. W–O bond lengths, are not reliable enough. Therefore, our model complex will greatly help to identify the structure, the electronic properties and the reaction mechanism at the tungstopterin active site.

The most characteristic structure of the model complex, **1** and **2a**, is the mutual *trans* influence between oxo and thiolate, which are both strong π-donors. For example, remarkably elongated sulfur–tungsten bonds were observed in the crystal structure described above. In the Raman spectra, the *trans* influence was also detected. ν(W=O) bands were found to be shifted to lower frequencies (ν_s = ca. 885 and ν_{as} = ca. 840 cm^{-1} shown in Table 4) than the bands in ordinary complexes (960—900 cm^{-1}).[30] The model studies on the oxidative reactions of the dioxomolybdenum(VI) complexes have revealed that the thiolate ligands are uniquely suitable for the activation of the oxo ligand.[18a,52] Therefore, in the tungsten enzyme, the active site oxo ligands are expected to be activated by the thiolate ligands of the dithiolene cofactor toward the specific oxidation reaction.

Chan et al.[54] have pointed out an important difference in the geometries of the models, **1** and **2a**, which make them distinct from the enzyme active site. Indeed, in the case of our model complex, **1**, the S–W–S bond angles between dithiolene ligands are 158.99(2)° (S2–W1–S4) and 85.52(2)° (S1–W1–S3). On the other hand, in the case of the tungsten cofactor, corresponding S–W–S bond angles are ca. 140° and ca. 110°.[21,54] These angles suggest the deformation of the geometry of W ion from Oh (= octahedron) to TP (= trigonalprism).

The theoretical calculations show that the Oh structure is more stable than the TP geometry, due to the repulsion between thiolates.[55] The preference of a TP geometry has generally been explained from the S···S bonding interaction between the thiolate ligands of tris(1,2-dithiolato) complexes. If there are repulsive interactions, the coordination will be changed to Oh or BCT from TP.[56] The enzyme active site should have some perturbation device to reduce the repulsion between thiolate ligands.

Chan et al.[54] also pointed out the energy differences of the molecular orbitals of the tungsten centers from these geometric differences which will affect the activation barrier for the oxo transfer process. We think that the structural difference between the models, **1** and **2a**, and the tungsten cofactor indicated the importance of "least stereochemical rearrangement" in the oxo transfer reaction to realize an efficient reactivity of the enzyme.[53]

There will be little or no movement of the ligating sulfur atoms in the oxo-transfer reaction process, if the reduced state has square pyramidal geometry like a W(IV) model complex, $(NEt_4)_2[W^{IV}O(bdt)_2]$ (**6**). "Least stereochemical rearrangement" of the ligating sulfur atoms facilitates oxo-transfer without requiring considerable reorganization of the tungsten cofactor. A specific device at the protein active site probably realizes such an unusual geometry. Similar small geometrical change in the electron transfer redox reaction have been discussed for an electron transfer enzyme, plastocyanin.[57]

The Activation and Stabilization of Oxo Ligands by the Tungstopterin and Molybdopterin at the Enzyme Active Site. From the model structure, we will propose the controlling mechanism of the *trans* influence between oxo and thiolate as a switching device of oxo-transfer reaction.

The X-ray absorption analysis of oxidized sulfite oxidase has demonstrated the presence of two terminal oxygen atoms at 1.68 Å, three sulfur atoms at 2.41 Å, one nitrogen or oxygen atom at 2.19 Å and one long sulfur atom at 2.86 Å.[26] The long sulfur has been considered to come from a single Mo–S(methionine) interaction. The presence of the two longer thiolate (2.60 Å) trans to the terminal oxo group in **1** supports the possibility that the long sulfur in native molybdooxidases is assignable to one thiolate of pterin dithiolene *trans* to the terminal oxo or sulfide group. When the pterin-dithiolene ligand coordinates as a thioketone-like sulfur ligand to Mo(VI) in the oxidized state, for example, in sulfite oxidase, the weak Mo–S π-interaction by the thioketonic ligand contributes to the stabilization of $O{=}Mo^{VI}$ bond trans to the thiolate ligand atom.

A large variety of molybdopterin cofactors containing pterin and phosphate groups have been isolated and characterized.[18—20] Redox active pterin-dithiolene group has been considered to be involved in the oxidation reaction. Actually, Garner et al.[58] reported electrochemical behavior of $[CpCo^{III}(S_2C_2H(quinoxalin\text{-}2\text{-}yl))]$, which contains a redox active pyrazine ring with a dithiolene substituent as model of the cofactor, and demonstrated how reduction at the metal

center may be coupled to the protonation of the pyrazine ring. From the model study, they have suggested the possibility of redox cooperativity between the molybdenum ion and the pterin dithiolene ligand.[58] If the oxidized enzyme has a thioketone form in the molybdopterin cofactor, the weak Mo–S(thioketonic sulfur) stabilize the *trans* Mo=O group as shown in Fig. 9. This is supported by the coodinaiton of thioketone-like thiolate ligand with large conjugated group in **1** as described above. When the molybdopterin cofactor has changed to have a thiolato sulfur ligand, the Mo–S π-bonding become strong. Then M^{VI}=O (M = W and Mo) bonding is activated toward an oxo-transfer reaction.

Conclusion

The crystal structure of $(NEt_4)_2[W^{VI}O_2(ndt)_2]\cdot H_2O$ (**1**) provided the detailed structural dimensions of the mutual *trans* influence between oxo and thiolate. The S–C bond distances of the thiolato ligands trans to terminal oxo groups are shorter than those at the *cis* positions. The partial double bonding at the S–C weakens π-bonding character of the Mo–S bonds *trans* to the oxo ligands and contributes to the stabilization of dioxotungsten(VI) having two thiolato ligands at the *trans* positions. In the case of tungsten and molybdenum oxidoreductases, the dithiolene ligand of molybdopterin can also stabilize the terminal oxo (or sulfide) ligands in the oxidized W(VI) and Mo(VI) states.

We are grateful for financial supports by JSPS Fellowships (H.O.; No. 1278 (1993—1995), No. 2947 (1995—1997)), and by a Grant-in-Aid for Specially Promoted Research from the Ministry of Education, Science, Sports and Culture (A.N., No. 06101004).

References

1) Y. Yamamoto, T. Saiki, S.-M. Liu, and L. G. Ljungdahl, *J. Biol. Chem.*, **258**, 1826 (1983).

2) H. White, R. Feicht, C. Huber, F. Lottspeich, and H. Simon, *Biol. Chem. Hoppe-Seyler*, **372**, 999 (1991).

3) S. P. Cramer, C. Liu, L. E. Mortenson, J. T. Spence, S. Liu, I. Yamamoto, and L. G. Ljungdahl, *J. Inorg. Biochem.*, **23**, 119 (1985).

4) H. White, G. Strobl, R. Feicht, and H. Simon, *Eur. J. Biochem.*, **184**, 89 (1989).

5) R. A. Schmitz, Richter, D. Linder, and R. K. Thauer, *Eur. J. Biochem.*, **207**, 559 (1992).

6) S. Mukund and M. W. W. Adams, *J. Biol. Chem.*, **265**, 11508 (1990).

7) S. Mukund and M. W. W. Adams, *J. Biol. Chem.*, **266**, 14208 (1991).

8) J. L. Johnson, K. V. Rajagopalan, S. Mukund, and M. W. W. Adams, *J. Biol. Chem.*, **268**, 4848 (1993).

9) M. W. W. Adams, *Adv. Inorg. Biochem.*, **38**, 341 (1992).

10) S. Mukund and M. W. W. Adams, *J. Biol. Chem.*, **268**, 13592 (1993).

11) R. Wanger and J. R. Andreesen, *Arch. Microbiol.*, **147**, 295 (1987).

12) J. B. Jones and T. C. Stadtman, *J. Biol. Chem.*, **256**, 656 (1981).

13) A. Juszczak, S. Aono, and M. W. W. Adams, *J. Biol. Chem.*, **266**, 13834 (1991). (Enzymes have not been identifed. The requirement of tungstate was reported for the bacterium growth. Tungsten enzyme is thus expected in this case.)

14) J. C. Deaton, E. I. Solomon, G. D. Watt, P. J. Wetherbee, and C. N. Durfor, *Biochem. Biophys. Res. Commun.*, **149**, 424 (1987).

15) G. N. George, R. C. Prince, S. Mukund, and M. W. W. Adams, *J. Am. Chem. Soc.*, **114**, 3521 (1992).

16) G. N. George, Y. Gea, R. C. Prince, S. Mukund, and M. W. W. Adams, *J. Inorg. Biochem.*, **43**, 241 (1991).

17) G. N. George, C. A. Kipke, R. C. Prince, R. A. Sunde, J. H. Enemark, and S. P. Cramer, *Biochemistry*, **28**, 5075 (1989).

18) a) S. P. Cramer, J. L. Johnson, A. A. Ribeiro, D. S. Millington, and K. V. Rajagopalan, *J. Biol. Chem.*, **262**, 16357 (1987); b) J. L. Johnson, J. L. Bastian, and K. V. Rajagopalan, *Proc. Natl. Acad. Sci. U.S.A.*, **87**, 3190 (1990); c) G. Borner, M. Karrasch, and R. K. Thauer, *FEBS Lett.*, **290**, 31 (1991).

19) R. A. Schwitz, M. Richter, D. Linder, and R. K. Thauer, *Eur. J. Biochem.*, **207**, 559 (1992).

20) J. L. Johnson, K. V. Rajagopalan, S. Munkund, and M. W. W. Adams, *J. Biol. Chem.*, **268**, 4848 (1993); b) R. A. Schmitz, M. Richter, D. Linder, and R. K. Thauer, *Eur. J. Biochem.*, **207**, 559 (1992).

21) M. K. Chan, S. Mukund, A. Kletzin, M. W. W. Adams, and D. C. Rees, *Science*, **267**, 1463 (1995).

22) N. Ueyama, H. Oku, and A. Nakamura, *J. Am. Chem. Soc.*, **114**, 7310 (1992).

23) a) S. Gruber, L. Kilpatrick, N. R. Bastian, K. V. Rajagopalan and T. G. Spiro, *J. Am. Chem. Soc.*, **112**, 8180 (1990); b) L. Kilpatric, K. V. Rajagopalan, J. Hilton, N. R. Bastian, E. I. Stiefel, R. S. Pilato, and T. G. Spiro, *Biochemistry*, **34**, 3032 (1995).

24) a) N. Benson, J. A. Farrar, A. G. McEwan, and A. J. Thomson, *FEBES Lett.*, **307**, 169 (1992); b) M. G. Finnegan, J. Hilton, K. V. Rajagopalan, and M. K. Johnson, *Inorg. Chem.*, **32**, 2616 (1993).

25) G. N. George, W. E. J. Cleland, J. H. Enemark, B. E. Smith, C. A. Kipke, S. A. Roberts, and S. P. Cramer, *J. Am. Chem. Soc.*, **112**, 2541 (1990).

26) J. M. Berg, K. O. Hodgson, S. P. Cramer, J. L. Corbin, A. Elseberry, N. Pariyadath, and E. I. Stiefel, *J. Am. Chem. Soc.*, **101**, 2774 (1979).

27) C. A. Rice, P. M. H. Kroneck, and J. T. Spence, *Inorg. Chem.*, **20**, 1996 (1981).

28) J. R. Bradbury, A. F. Masters, A. C. McDonell, A. A. Brunette, A. M. Bond, and A. G. Wedd, *J. Am. Chem. Soc.*, **103**, 1959 (1981).

29) G. R. Hanson, A. A. Brunette, A. C. McDonell, K. S. Murray, and A. G. Wedd, *J. Am. Chem. Soc.*, **103**, 1953 (1981).

30) S. Yu and R. H. Holm, *Inorg. Chem.*, **28**, 4385 (1989).

31) R. H. Holm, *Chem. Rev.*, **87**, 1401 (1987).

32) A. Cervilla, E. Llopis, A. Ribera, A. Doménech, and E. Sinn, *J. Chem. Soc., Dalton Trans.*, **1994**, 3511.

33) A. A. Eagle, S. M. Harven, E. R. Tiekink, and C. G. Young, *J. Am. Chem. Soc.*, **116**, 9749 (1994).

34) S. K. Das, P. K. Chaudhury, D. Biswas, and S. Sarkar, *J. Am. Chem. Soc.*, **116**, 9061 (1994); S. K. Das, D. Biswas, R. Maiti, and S. Sarkar, *J. Am. Chem. Soc.*, **118**, 1387 (1996).

35) G. D. Figuly, C. K. Loop, and J. C. Martin, *J. Am. Chem. Soc.*, **111**, 654 (1989); E. Block, V. Eswarakrishnan, M. Gernon, G. Ofori-Okai, C. Saha, K. Tang, and J. Zubieta, *J. Am. Chem. Soc.*, **111**, 658 (1989).

36) D. T. Cromer and J. T. Waber, "International Tables for X-

Ray Cryatallography," The Kynoch Press, Birmingham, England (1974), Vol. IV, Table 2.2A and Table 2.3.1.

37) A. Dedieu, T. A. Albright, and R. Hoffmann, *J. Am. Chem. Soc.*, **101**, 585 (1979).

38) M. M. L. Chen and R. Hoffmann, *J. Am. Chem. Soc.*, **98**, 1647 (1976); N. T. Anh, M. Elian, and R. Hoffmann, *J. Am. Chem. Soc.*, **110**, 110 (1978).

39) E. I. Stiefel, K. F. Miller, A. E. Bruce, N. Pariyadath, J. Heinecke, J. L. Corbin, J. M. Berg, and K. O. Hodgson, "Molybdenum Chemistry of Biological Significance," ed by S. Otsuka and W. E. Newton, Plenum Press, New York (1980), p. 279.

40) S. Boyde, C. D. Garner, J. A. Joule, and D. J. Rowe, *J. Chem. Soc., Chem. Commun.*, **1987**, 800.

41) H. Oku, N. Ueyama, and A. Nakamura, *Chem. Lett.*, **1994**, 607.

42) H. Oku, N. Ueyama, and A. Nakamura, *Inorg. Chem.*, **34**, 3667 (1995).

43) a) N. Ueyama, H. Oku, T. Okamura, N. Yoshinaga, and A. Nakamura, *Inorg. Chem.*, **35**, 643 (1996); b) N. Yoshinaga, N. Ueyama, T. Okamura, and A. Nakamura, *Chem. Lett.*, **1990**, 1655.

44) N. Ueyama, T. Sugawara, K. Sasaki, A. Nakamura, S. Yamashita, Wakatsuki, H. Yamazaki, and N. Yasuoka, *Inorg. Chem.*, **27**, 741 (1988).

45) a) K. Jug, *J. Comput. Chem.*, **5**, 555 (1984); b) K. B. Wiberg, *Tetrahedron*, **24**, 1083 (1968).

46) L. J. DeHayes, H. C. Faulkner, W. H. Doub, Jr., and D. T. Sawyer, *Inorg. Chem.*, **14**, 2110 (1975).

47) P. Subramanian, S. Burgayer, S. Richards, V. Szalaki, and T. G. Spiro, *Inorg. Chem.*, **29**, 3849 (1990).

48) R. M. Badger, *J. Chem. Phys.*, **3**, 710 (1935); D. R. Hershbach and V. W. Laurie, *J. Chem. Phys.*, **35**, 458 (1961).

49) H. Oku, N. Ueyama, and A. Nakamura, *Chem. Lett.*, **1995**, 621.

50) $P_\pi(W_\pi\text{–}S_\pi)$ and $P_\pi(Wd_\pi\text{–}Sd_\pi)$ include the components of $Wd_\delta\text{–}Sd_\delta$ interaction, but these are small and negligible in each overlap population value.

51) K. Tatsumi, Y. Inoue, H. Kawaguchi, M. Kohsaka, A. Nakamura, R. E. Cramer, W. VanDoorne, G. J. Tagoshi, and P. N. Richman, *Organometallilcs*, **12**, 352 (1993).

52) J. Topich and J. T. Lyon, III, *Inorg. Chem.*, **23**, 3202 (1984).

53) H. Oku, N. Ueyama, and A. Nakamura, *Chem. Lett.*, **1996**, 31.

54) M. K. Chan, M. W. W. Adams, D. C. Rees, private communication.

55) By the ab initio calculation, the geometry optimization was carried out for the trigonal prismatic (C_{2v}) and the octahedral (C_2) structure of $[Mo^{VI}O_2(1,2\text{-ethylenedithiolato})_2]^{2-}$ with 3-21G* basis sets and Hartree–Fock approximation. As a result, $E = -5841.1710754$ a.u. for the trigonal prism structure and -5841.2142870 a.u. for the octahedral structure. A lower energy value ($\Delta E = -27.0978$ kcal mol^{-1}) was obtained for the octahedral structure.

56) K. Tatsumi, I. Matsubara, Y. Inoue, A. Nakamura, K. Miki, and N. Kasai, *J. Am. Chem. Soc.*, **111**, 7766 (1989).

57) J. E. Huheey, "Inorganic Chemistry," 3rd ed, Harper & Row, Cambridge (1983), p. 867.

58) C. D. Garner, E. M. Armstrong, M. J. Ashccroft, M. S. Austerberry, J. H. Birks, D. Collison, A. Goodwin, L. Larsen, D. J. Rowe, J. R. Russel, in "Molybdenum Enzymes, Cofactors, and Model Systems," ed by E. I. Stiefel, D. C. Coucouvanis, and W. E. Newton, American Chemical Society, Washington DC (1993).